

---

## The dynamics of heat lows over elevated terrain

Roger K. Smith<sup>a\*</sup> and Thomas Spengler<sup>b</sup>

<sup>a</sup>*Meteorological Institute, University of Munich, Germany*

<sup>b</sup>*Atmospheric and Oceanic Sciences Program, Princeton University, New Jersey, USA*

\*Correspondence to: Roger K. Smith, Meteorological Institute, University of Munich, Theresienstrasse 37, 80333 Munich, Germany. E-mail: roger.smith@lmu.de

---

Orographic effects on the dynamics of heat lows are investigated in an idealized flow configuration using a hydrostatic numerical model. The behaviour of the heat low that forms over a plateau-like orography on a circular island is compared with that when the island is flat, and that when the plateau is surrounded by land instead of sea. In all cases, a broad-scale, negative radial gradient of potential temperature forms in the daytime mixed layer over land. The presence of orography enhances the broad-scale baroclinicity over the orographic slope due to the identical heating of a column of air with a reduced mass, i.e. lower surface pressure. In the absence of sea, the baroclinicity is solely confined to the slope of the orography. The broad-scale potential temperature gradient results in an overturning circulation in the lowest few kilometres, which is separate from the shallower and more intense sea breeze circulation in the island cases. The presence of orography leads to a stronger overturning circulation via enhanced baroclinicity. In the case without sea, both the overturning circulation and tangential circulation are closely tied to the orography. The overturning circulation advects absolute angular momentum inwards to spin up the low-level circulation, despite some frictional loss of angular momentum en route. During the night, radiative cooling over the land leads to a strong nocturnal low-level jet that amplifies the spin-up process. During the daytime, the cyclone weakens as the angular momentum is convectively mixed through a deep layer. The study extends an earlier one of Reichmann and Smith and corrects some details in their model. The results offer a refined interpretation of the Atlantic inflow to the Saharan heat low, described recently by Grams *et al.*, and emphasize the role of orography in the formation of the inland baroclinic zone, which is a feature thereof. Copyright © 2011 Royal Meteorological Society

*Key Words:* heat trough; thermal low; thermal trough; radiation scheme; baroclinic zone; orography

*Received 26 July 2010; Revised 28 October 2010; Accepted 29 October 2010; Published online in Wiley Online Library 12 January 2011*

*Citation:* Smith RK, Spengler T. 2011. The dynamics of heat lows over elevated terrain. *Q. J. R. Meteorol. Soc.* 137: 250–263. DOI:10.1002/qj.737

### 1. Introduction

Heat lows or troughs are a prominent climatological feature of many arid land areas of the world during the warmer months, especially in the Subtropics when insolation is at its peak. Such regions include northern and southwestern Africa, northwestern and northeastern

Australia, the Arabian peninsula, west Pakistan and northern India, the Qinghai-Xizang plateau in China, southwestern North America, and the Iberian peninsula. A list of references to studies of the heat lows in these regions is given by Rácz and Smith (1999), henceforth RS99. Some authors refer to these systems as thermal lows or thermal troughs (e.g. Johnson, 2003). Recently, there has been a renewed

focus on heat lows as a result of the African Monsoon Multidisciplinary Analysis programme (AMMA), which was designed to improve our understanding of the West African summer monsoon (Redelsperger *et al.*, 2006; Lafore *et al.*, 2010). Research during the last decade has pointed to the important role of the Saharan heat low in the maintenance of the African easterly jet, which is a major feature of the monsoon (Thorncroft and Blackburn, 1999), and on the dynamics of the monsoon itself (Parker *et al.*, 2005). There has been interest also in the Iberian heat low (Hoinka and Castro, 2003).

Heat lows or troughs are shallow disturbances, generally confined below a height of 3 km, but they may extend to 5 km when surface heating is particularly intense, as over West Africa in summer. Heat lows and heat troughs have many dynamical features in common<sup>†</sup>, the main difference being the more prominent role of horizontal deformation in the heat trough, where the vertical component of vorticity is dominated by the shear component. The distinction in a surface isobaric chart can depend on the isobar spacing, where the former has at least one closed isobar while the latter has the form of an open wave.

Over the last three decades, there have been several numerical modelling studies of heat lows, some in idealized flow configurations (Leslie, 1980; Fandry and Leslie, 1984; Adams, 1986, 1993; Kepert and Smith, 1992; Gaertner *et al.*, 1993; Rácz and Smith, 1999; Reichmann and Smith, 2003; Spengler *et al.*, 2005; Zängl and Chico, 2006; Spengler and Smith, 2008) and others related to the heat low in specific regions (Alonso *et al.*, 1994; Leslie and Skinner, 1994; Portela and Castro, 1996; Hoinka and Castro, 2003; Grams *et al.*, 2010). Zängl and Chico (2006) focused on the heat low over high elevated terrain surrounded only by land.

The numerical study by RS99 sought to understand the fundamental dynamical processes of the heat low that forms over a flat square island when the island is subjected to a diurnal cycle of radiative heating and cooling. In the model, the cycle of heating and cooling of the atmosphere was accomplished using the Mellor–Yamada  $2\frac{1}{4}$  parametrization scheme for the boundary layer in association with the surface heating or cooling. The ground temperature over land was diagnosed from a surface heat balance condition and the sea-surface temperature was held constant. It was shown that the heat low has a minimum surface pressure in the late afternoon or early evening following strong insolation of the land, while the relative vorticity and low-level winds are strongest in the early morning hours following a prolonged period of low-level convergence associated with the formation of a nocturnal low-level jet. Thus the heat low is not approximately in quasi-geostrophic balance or gradient wind balance. The strengthening of the low-level

cyclone over night is associated with the Coriolis turning of the jet. A few hours after sunrise, deep convective mixing destroys the jet and the cyclonic flow weakens.

RS99 showed further that, although a cyclonic vortex, the heat low is characterized by an anticyclonic potential vorticity anomaly relative to its environment on account of the greatly reduced static stability in the convectively well-mixed boundary layer. As a result of this reduced static stability, the horizontal components of relative vorticity and horizontal potential temperature gradient make a non-negligible contribution to the potential vorticity in the mixed layer. They investigated also the effects of different island sizes and of latitude on various aspects of the heat low, but gave little attention to the overlying anticyclone. It was shown that many of the basic features of the circulation, such as the ageostrophic effects associated with the coastal sea breezes and the nocturnal low-level jet, were similar to those observed in the inland heat trough over northeastern Australia (e.g. Preissler *et al.*, 2002). These features have been found subsequently to explain important aspects of the West African Monsoon system and the Saharan heat low (Parker *et al.*, 2005).

A subsequent paper (Reichmann and Smith, 2003, henceforth RS03), examined the effects of orography on heat low formation and structure. After long integration times, the heating scheme in the RS99 model leads to unrealistic mixed-layer depths because the only mechanism for cooling to oppose the net heating of the atmosphere is that which occurs in a shallow layer adjacent to the surface. In an effort to remove this limitation, RS03 incorporated the radiation scheme proposed by Raymond (1994) in the model and showed that its implementation leads to a more realistic depth of the daytime mixed layer. The scheme is based on a grey atmosphere approximation and allows the atmosphere to cool, thereby preventing the long-term growth of the mixed-layer depth.

The RS99 model was extended further by Spengler *et al.* (2005) to investigate the effects of simple basic flows on the dynamics of heat lows. During the course of their study, they discovered some errors in the model initialization and in the numerical implementation of the radiation scheme by RS03 as well as errors in Raymond (1994). These errors are documented in Appendix A. Fortunately they were found to have only a small effect on the results presented by RS03. Nevertheless, their discovery led Spengler and Smith (2008), henceforth SS08, to develop an improved, higher-resolution version of the RS99 model that included a revised and corrected version of Raymond's radiation scheme. The new model was used to study the heat low that develops over a circular flat island, a slightly simpler configuration than the square island studied by RS99 and Spengler *et al.* (2005).

SS08 used their new model to investigate aspects of the dynamics of heat lows not previously touched upon by RS99, including the development of an upper-level anticyclone and the degree to which the cyclonic and anticyclonic circulations are in gradient wind balance. In particular, they showed that the anticyclone extends through much of the troposphere, but has its maximum strength in the lower troposphere, just offshore. It exhibits relatively little diurnal variation when the heat low reaches its mature stage – much less so than the low-level cyclone. The anticyclone develops steadily over a period of a few days and is associated with the return (offshore) branch of the sea breeze circulation in the lower troposphere, and with a slow diurnal-mean outflow in the

<sup>†</sup> At extreme ends of the idealization, many aspects of an axisymmetric heat low are isomorphic to those of a two-dimensional trough. Both types of disturbance may be thought of as low-level cyclonic relative vorticity maxima that are linked to horizontal gradients of diabatic heating. One important difference between these extremes is the fact that the absolute angular momentum in the axisymmetric case involves radius times the transverse velocity, while in the two-dimensional case it involves only the linear transverse velocity component. Even when absolute angular momentum is only partially conserved, this distinction has important quantitative implications. These implications were discussed in a moist context by Ulrich *et al.* (2002), who examined the differences between system intensification in a simple two-dimensional model for the intertropical convergence zone and an axisymmetric model for a tropical cyclone.

middle and upper troposphere. The outflow at upper levels may be interpreted as a mean drift induced by upward-propagating inertia-gravity waves that are initiated by the inland penetrating sea breeze front during the afternoon and evening.

Unlike the heat low, the upper anticyclone is largely in gradient wind balance, except in the neighbourhood of this gravity wave. The gravity wave has a significant effect on the radial and vertical components of the motion field at any one time and time averaging is required to isolate the more steady parts of these components.

SS08 showed that, in a mean sense, one can distinguish between distinct patterns of the tangential flow component:

- between midnight and noon, when the low-level cyclone is strongest, and
- between noon and midnight when it is much weaker.

These differences reflect the strong turbulent mixing of momentum in the mixed layer over land during the afternoon, which leads to a significant weakening of the cyclone, and the formation of a strong low-level jet at night, which re-amplifies the cyclone circulation.

In this article we revisit the study of RS03 using the improved model developed by SS08. The main focus is to describe and understand the differences between calculations with and without orography, with a variety of orographic shapes, and with orography, with or without a surrounding sea. We examine also the structure of the upper-level anticyclone and its diurnal variation in the presence of orography.

The article is structured as follows. In section 2 we describe briefly the numerical model and the configuration of the topography. Section 3 details the experiments carried out and the results are presented in section 4. The conclusions are given in section 5.

## 2. Model description

The numerical model is identical to the three-dimensional, hydrostatic, primitive-equation model described in detail by SS08. It differs from that used by RS03, the three main changes being the improvement and correction of the radiation scheme, the inclusion of a relaxation scheme for the horizontal boundary conditions, and the inclusion of ten additional upper model levels with increased horizontal diffusion to reduce the reflection of gravity waves from the top of the domain.

The model is formulated in sigma-coordinates on a Northern Hemisphere  $f$ -plane centred at 20°N latitude. The equations are expressed as finite differences on a domain with 40 interior  $\sigma$ -levels on a non-staggered, Arakawa A-Grid in the horizontal directions. There are  $199 \times 199$  grid points in the horizontal with a grid spacing of 25 km, which give a total domain size 4950 km west to east and south to north. Heat diffusion in the soil is calculated using a three-layer soil model. The Mellor–Yamada  $2\frac{1}{4}$  boundary layer parametrization (Mellor and Yamada, 1974, 1982) is used to represent turbulent mixing in the atmosphere and an idealized radiation scheme is used to calculate atmospheric heating due to long and short wave radiation (SS08 give details).

The model configuration comprises a circular island with a radius of 800 km from the centre of the domain. The surrounding sea has a constant sea-surface temperature of

24 °C, except in one case, where it is 20 °C. In some of the experiments described, the orography has the form of a plateau while in others it rises sharply to a peak near the centre of the island. The terrain height in all cases is given by the formula:

$$h(r) = h_0 \exp \left\{ -0.5 \left( \frac{r}{r_0} \right)^n \right\}, \quad (1)$$

where  $r$  is the distance (km) from the domain centre and  $h_0$ ,  $r_0$  and  $n$  are constants. These constants are detailed in Table I.

The calculations are begun from a state in which the atmosphere is at rest with a temperature sounding that is in radiative-convective equilibrium. This sounding is derived from a one-dimensional version of the model. At the initial time (0600 h local time on day 1), the sun is switched on and a diurnal cycle of heating and cooling ensues. The flow induced by this cycle reaches a quasi-steady state after 11 d. We focus here entirely on this quasi-steady cycle and do not discuss the spin-up process, which is similar to that described by SS08.

## 3. The numerical experiments

A series of ten numerical experiments are discussed. These are listed in Table I. The island experiments have different orographic shapes, characterized by different constants in Eq. (1) as detailed in Table I. The control experiment (Experiment IS) is where the island is flat. The three main experiments with orography are those with a Gaussian-shaped orography (Experiment G), with a plateau (Experiment PS) and with the same plateau shape as in Experiment PS, but surrounded by an area of flat land instead of sea (Experiment PNS). Three further experiments were carried out: one for an extra-narrow Gaussian-shaped terrain (Experiment G2); one for a wide plateau (Experiment WP); and one an extra-wide plateau (Experiment WP2). These were designed to further investigate the effects of the plateau width and the results from them will be touched upon briefly. The maximum height of the orography,  $h_0$ , in all of these experiments is 600 m. The various orographic profiles are shown in Figure 1. The profiles in Experiments PS and PNS are similar to those used by RS03<sup>‡</sup>.

Three final experiments are discussed in which the height of the plateau is reduced to 200 m. The orographic profile is shown also in Figure 1. Experiments SPS and SPNS are otherwise identical to Experiments PS and PNS, respectively. Experiment GR is similar to Experiment SPS, but has steeper orography, a broader coastal plain and a sea-surface temperature of 20 °C, similar to the configuration relevant to the Saharan heat low used by Grams *et al.* (2010).

<sup>‡</sup>The constants chosen for the orography in Experiments PS, PNS, WP, and G differ slightly from those used by RS03 (PS and PNS:  $r_0 = 480$  km and  $n = 4$ , WP:  $r_0 = 640$  km,  $n = 8$ , G:  $r_0 = 400$  km,  $n = 2$ ). The reason for the change is to minimize numerical issues with the jump in orographic height at the coast. These jumps are now much less than the depth of the first model level above the sea, i.e. about 30 m. The coastal step is a maximum for Experiment WP, being  $\approx 9$  m.

Table I. Numerical experiments discussed in the text.

| Experiment | Description           | $r_0$ (km) | $n$ | $h_0$ (m) | Sea |
|------------|-----------------------|------------|-----|-----------|-----|
| IS         | Flat island           | –          | –   | 0         | yes |
| G          | Gaussian              | 250        | 2   | 600       | yes |
| PS         | Plateau               | 450        | 4   | 600       | yes |
| PNS        | Plateau without sea   | 450        | 4   | 600       | no  |
| WP         | Wide plateau          | 600        | 8   | 600       | yes |
| G2         | Extra-narrow Gaussian | 125        | 2   | 600       | yes |
| WP2        | Extra-wide plateau    | 700        | 16  | 600       | yes |
| SPS        | Shallow plateau       | 450        | 4   | 200       | yes |
| SPNS       | Shallow plateau       | 450        | 4   | 200       | no  |
| GR         | Grams (SST = 20 °C)   | –          | –   | 200       | yes |

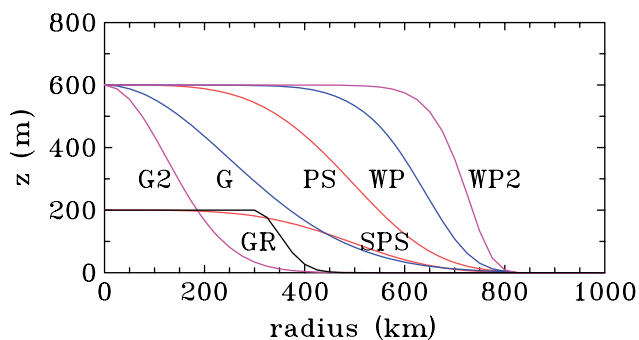


**Figure 1.** Radius–height profiles of the orography in Experiments G, G2, PS, WP, WP2, SPS, GR. The profiles for Experiments PNS and SPNS are the same as those of Experiments PS and SPS, respectively. The profile for Experiment GR is similar to that of the shallow plateau, SPS, but has steeper orography and a broader coastal plain. This figure is available in colour online at [wileyonlinelibrary.com/journal/qj](http://wileyonlinelibrary.com/journal/qj)

#### 4. The effects of orography

##### 4.1. Thermal field

As a step towards elucidating the effects of orography, we begin by comparing height–radius<sup>§</sup> cross-sections of potential temperature,  $\theta$ , at selected times (1800 h and 0600 h) in the first four experiments (IS, G, PS and PNS) in Table I. These cross-sections are shown in Figure 2. In each case, at 1800 h, there is a well-mixed layer over the land that has a broad-scale negative radial gradient of  $\theta$ . In the first three experiments, there is a locally large radial gradient of  $\theta$  in a shallower layer near the coast, which is associated with the surface temperature discontinuity at the coast and marks the sea breeze front. The radial gradients of  $\theta$  are highlighted in Figure 3, which shows the radial profiles of  $\theta$  at a height of 1500 m (well above the surface) for the seven experiments with a 600 m high plateau at this time. In all the island experiments with orography, the mixed-layer  $\theta$  at the centre of the island is approximately 3 K larger than in Experiment IS.

Comparing Figures 1 and 3 suggests that the radial gradient of  $\theta$  is approximately the sum of two components. The first component is the negative radial gradient over flat land associated with the fact that the temperature

progressively adjusts from the state of radiative-convective equilibrium over the sea to radiative-convective equilibrium over dry land with increasing distance inland from the coast. The second component is the orographic contribution that arises because the mixed-layer  $\theta$  increases with increasing topographic elevation. We show in Appendix B that, as the height of the orography increases and the surface pressure decreases, the mixed-layer temperature increases monotonically because the surface heating is distributed over a column of lighter air. The two components combine to produce a broad-scale baroclinic zone over the land in which the radial gradient of  $\theta$  is enhanced over orographic slopes. During the night, a strong stable layer forms over the land in response to the radiative cooling of the surface, but a broad-scale baroclinic zone remains within the residual mixed layer.

There are significant differences in the potential temperature distribution when there is no sea surrounding the plateau (compare Figures 2(e, f) with Figures 2(g, h), respectively). In Experiment PNS, the air over the land is everywhere well mixed during the day and, without the tempering effect of the sea, the potential temperatures are everywhere much higher than in the island experiments. In this case the radial gradient of  $\theta$  is associated with the fact that the temperature seeks to adjust from a state of radiative-convective equilibrium over the plateau to radiative-convective equilibrium over flat land with increasing radius. The surface temperatures remote from the orography range between 38.7 °C and 46.9 °C compared with the sea-surface temperature of 24 °C in Experiment PS. Therefore, the radial gradient of potential temperature in Experiment PNS is smaller than that in Experiment PS and at 1800 h is mostly confined to the slope of the orography (Figure 2(g)) for reasons explained above.

At 0600 h the surface-based stable layer is a little deeper in Experiments G and PS, especially in the central part of the island not reached by the sea breeze (compare Figures 2(d, f) with Figure 2(b)).

Figure 4 shows a vertical profile of  $\theta$  over the sea at a radius of 1500 km, remote from land, in Experiment IS. This profile, which is typical of the other experiments, shows an unstable surface layer, a well-mixed layer above it, and a stably stratified layer above the mixed layer. This structure looks remarkably realistic, bearing in mind the simplicity of the radiation scheme. The decrease in  $\theta$  across the unstable layer corresponds with an air–sea temperature difference of 1.7 °C, which is within the observed range over the tropical ocean (e.g. Fitzjarrald and Garstang, 1981, their Figure 3)).

<sup>§</sup>Because the flows are essentially axisymmetric, we show all cross-sections in this form.

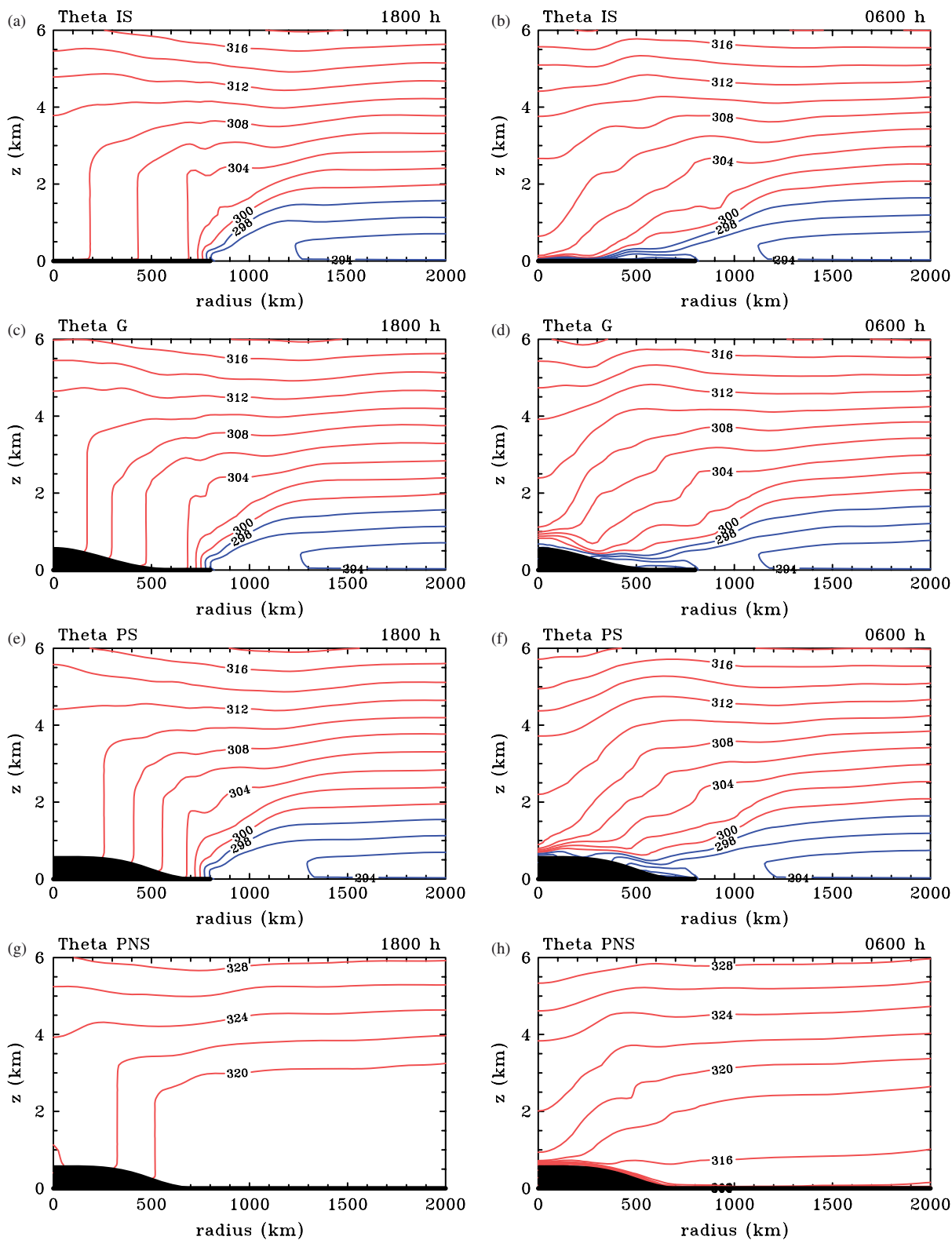


**Figure 2.** Radius–height cross-sections showing the isentropes of potential temperature at (a, c, e, g) 1800 h and (b, d, f, h) 0600 h in the experiments (a, b) IS, (c, d) G, (e, f) PS, and (g, h) PNS. The contour interval is 2 K. Contours with values less than 300 K, characteristic of air at low levels over the sea, are in bold (blue in the colour version). This figure is available in colour online at [wileyonlinelibrary.com/journal/qj](http://wileyonlinelibrary.com/journal/qj)

This profile shows little diurnal variation as the sea-surface temperature is held fixed over the diurnal cycle.

#### 4.2. Overturning circulation

The experiments with larger broad-scale radial gradients of  $\theta$  have stronger overturning circulations in the lowest few

kilometres, as may be inferred from the radial velocity fields shown in Figures 5(a–c) and the corresponding vertical velocity fields shown in Figures 6(a–c) at the same times as in Figure 2. A useful cartoon showing conceptually how the broad-scale circulation arises and illustrating the effects of advection by this circulation is given by Emanuel *et al.* (1994, their Figure 2).

Some notable features of the overturning circulation are as follows. In general, in all the experiments, the overturning circulation tends to be strongest in the region of largest radial temperature gradient, typically just behind the sea breeze front or above the orographic slope.

In the three island experiments (IS, G and PS), the low-level inflow at 1800 h has two maxima over the land. The inner one is clearly associated with broad-scale convergence induced by the broad-scale heating over the land, and the outer one, which is much stronger and located a little inland from the coast, is associated with the sea breeze. The sea breeze front has a prominent signature in the vertical velocity field also, with a relatively narrow sloping region of ascent just inland of an equally narrow sloping region of descent (Figures 6(a–c)). As discussed in SS08, the sea breeze initiates an upward-propagating inertia-gravity wave at its leading edge, the upward propagation being evident in the inward slope of the regions of ascent and subsidence with height. The gravity wave is a clear feature of animations of the vertical velocity field at 10 min intervals and, as shown in SS08, it is an important feature in the progressive growth of the upper-level anticyclone with height.

In Experiment G, the low-level inflow near the centre of the island is greatly enhanced during the afternoon by the anabatic flow on the orography compared with that in Experiment IS (compare Figures 5(a–c)). This difference persists during the night, but the depth of inflow collapses as the night progresses and the air near the surface stabilizes because of radiative cooling. In Experiment G, the double maximum persists and is still present at 0600 h (Figure 5(d)), but in Experiments IS and PS the inner maximum has disappeared and the flow near the island centre has weakened substantially compared with that in Experiment G. As shown below, these inflow maxima give rise to separate maxima in the low-level cyclonic circulation.

In Experiment PS, the slope of the orography is close enough to the coast that the sea breeze and anabatic up-slope flow rapidly merge (they are close to this point at 1800 h, as seen in Figure 5(e)). Thus for most of the evening and through the night, there is a single region of low-level inflow surmounted by a single region of outflow.

In the absence of sea (Experiment PNS), there is no sea breeze and the thermally induced inflow is associated with the anabatic flow on the slope. On account of the smaller radial gradient of  $\theta$  in this experiment, the inflow at 1800 h is much weaker than that in Experiment PS. At 0600 h the inflow is very shallow over the orography.

In all four experiments, the inflow over land and the layer of outflow above it become progressively shallower during the night. In particular, a shallow layer of outflow forms above the inflow near the coast (Figures 5(b, d, f, h)). The shallow nature of these flows are presumably related to the strong stabilization of the near-surface air over land during the night (Figures 2(b, d, f, h)).

In all four experiments (IS, G, PS, and PNS) there is mostly ascent over the land in the late afternoon (Figures 6(a, c, e, g)) and subsidence in the early morning (Figures 6(b, d, f, h)). The exceptions are in the upper troposphere and in a shallow region near the centre that is most prominent in Experiment PS where the layer of strong inflow turns upwards and then flows outwards.

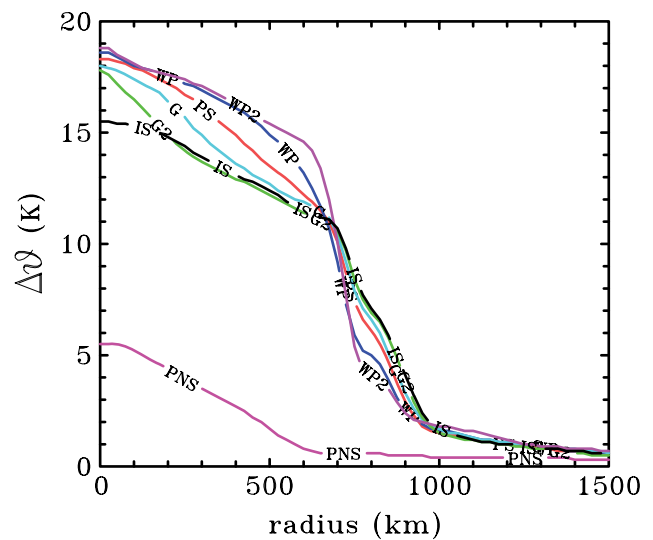


**Figure 3.** Radial profiles of the potential temperature difference,  $\Delta\theta$ , between the axis and far radial boundary at a height of 1500 m at 1800 h in the various experiments: IS, PS, PNS, WP, WP2, G and G2 (defined in Table I). This figure is available in colour online at [wileyonlinelibrary.com/journal/qj](http://wileyonlinelibrary.com/journal/qj)

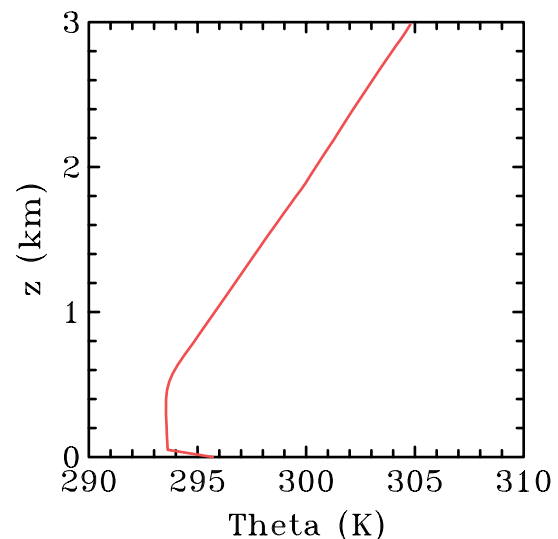


**Figure 4.** Vertical profile of the potential temperature,  $\theta$ , over the sea at a radius of 1500 km, remote from land, at 1800 h in Experiment IS. This figure is available in colour online at [wileyonlinelibrary.com/journal/qj](http://wileyonlinelibrary.com/journal/qj)

#### 4.3. Tangential circulation

As explained in SS08, the spin-up of the low-level cyclonic flow within the heat low is a result of the radial convergence of absolute angular momentum accompanying the inflow. The absolute angular momentum,  $M$  is defined by  $rv + fr^2/2$ , where  $r$  is the radius,  $v$  is the tangential wind component and  $f$  is the Coriolis parameter. Near the surface,  $M$  is not conserved on account of the frictional torque. Nevertheless, the convergence of  $M$  leads to spin-up if air parcels can be brought to small radii quickly enough, before losing an appreciable amount of  $M$  (Smith and Vogl, 2008; Smith *et al.*, 2009). An alternative, but equivalent interpretation for the spin-up of the cyclonic flow follows directly from Newton's second law in which the sole forces

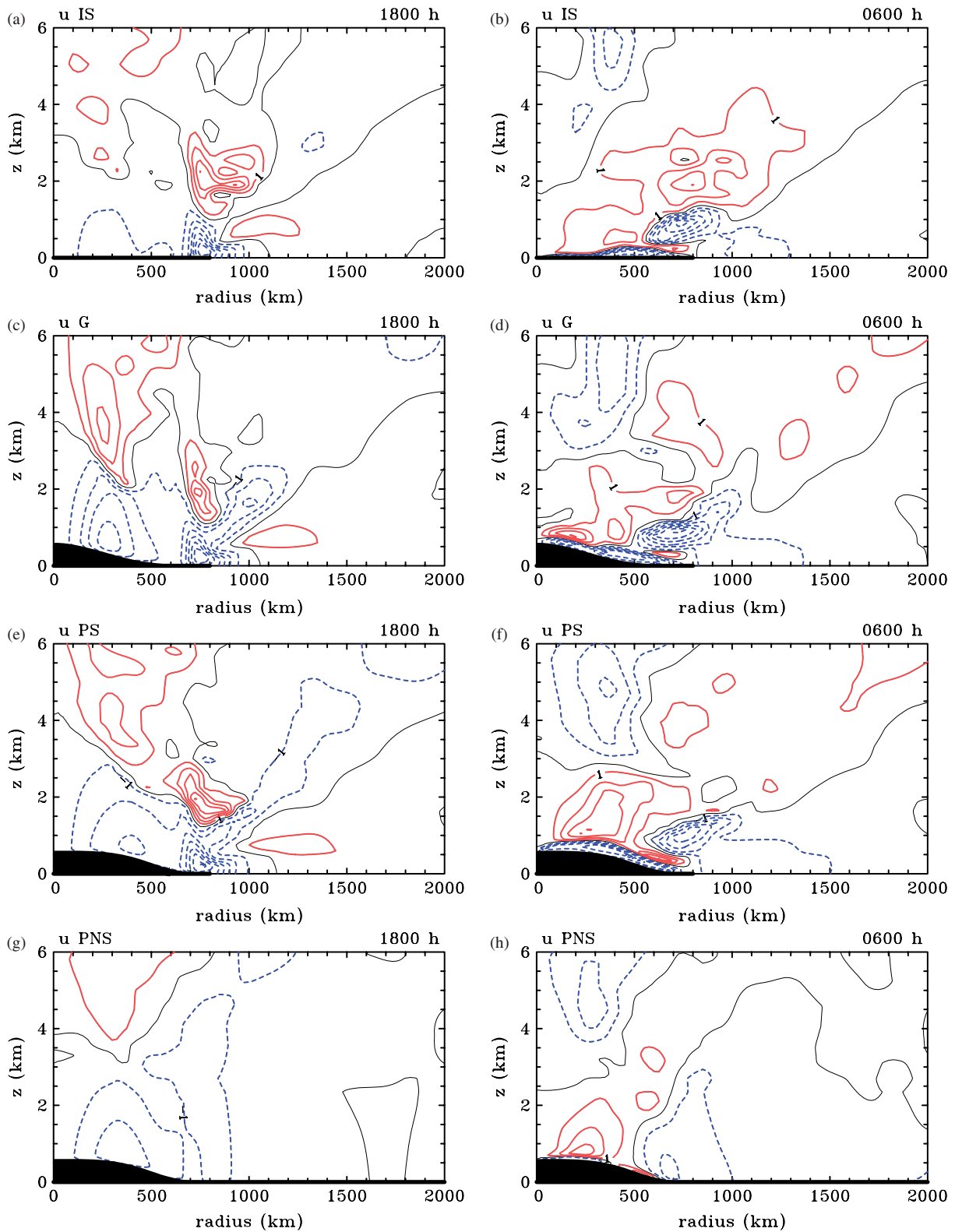


**Figure 5.** As Figure 3, but showing isotachs of the radial wind component. The contour interval is  $1 \text{ m s}^{-1}$ , with positive contours solid and negative contours dashed. This figure is available in colour online at [wileyonlinelibrary.com/journal/qj](http://wileyonlinelibrary.com/journal/qj)

are the generalized Coriolis force<sup>‡</sup> associated with the radial component of inflow and the azimuthal component of the frictional force. If the generalized Coriolis force exceeds the frictional force, the tangential winds will accelerate.

<sup>‡</sup>The generalized Coriolis force is  $-u(v/r + f)$ , where  $u$  is the mean radial velocity component.

As shown by RS99, the tangential wind component has a large diurnal variation in strength in the lower atmosphere. The stabilization of the near-surface air over land after sunset leads to the formation of a nocturnal low-level jet, which strengthens the low-level inflow and intensifies the low-level cyclone. During the afternoon, when the horizontal momentum that was generated by the thermally-induced

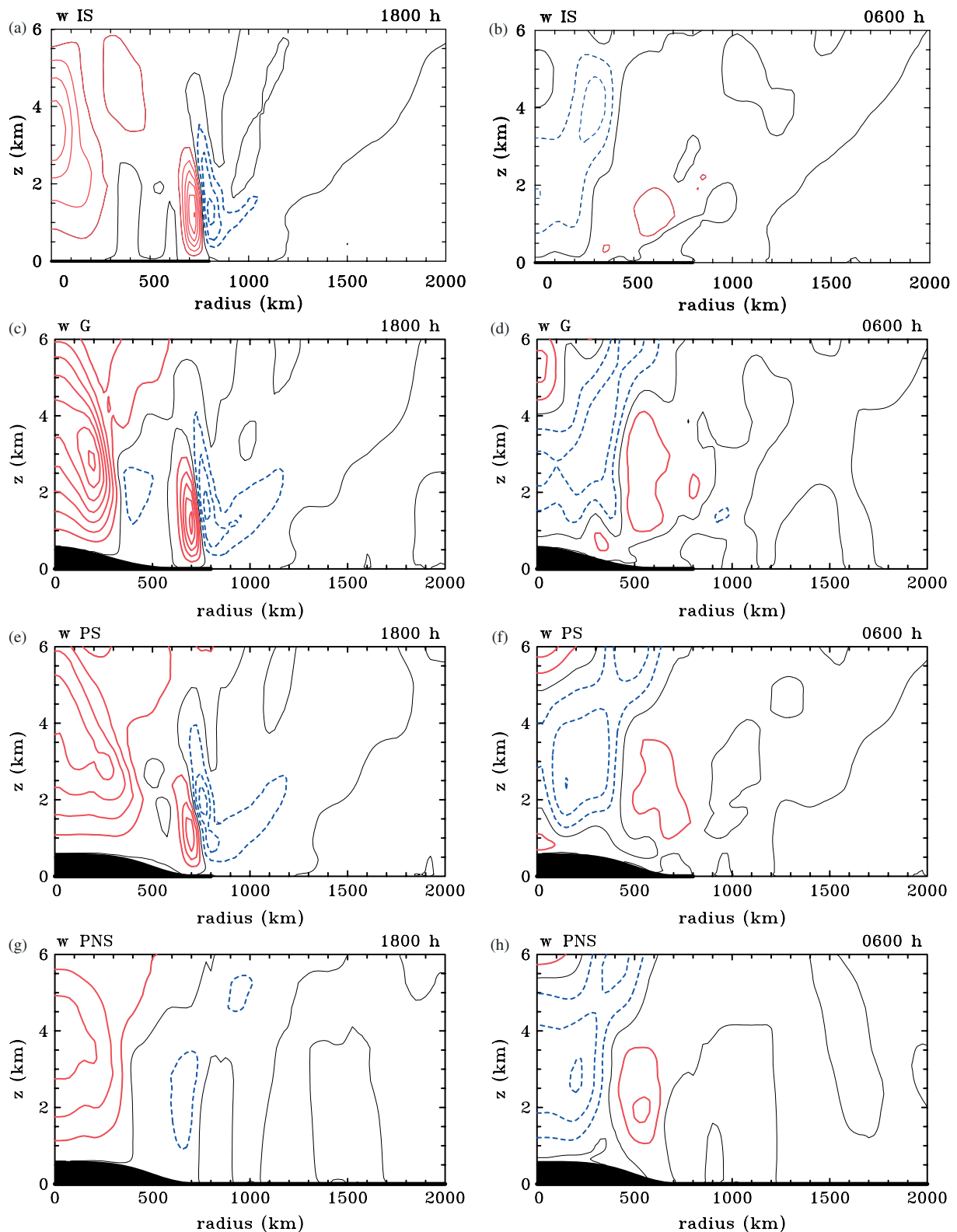


**Figure 6.** As Figure 3, but showing contours of the vertical velocity component. The contour interval is  $1 \text{ cm s}^{-1}$ , with positive contours solid and negative contours dashed. This figure is available in colour online at [wileyonlinelibrary.com/journal/qj](http://wileyonlinelibrary.com/journal/qj)

low-level inflow overnight has been distributed throughout the mixed layer, the cyclone is significantly weaker than it is in the early morning.

Figure 7 compares height–radius cross-sections of the tangential wind component at 1800 h and 0600 h in the four Experiments IS, G, PS and PNS. The latter time is the time of the maximum of this wind component in

Experiment IS: (Figure 6(b)). At 1800 h, maximum cyclonic wind speeds barely exceed  $4 \text{ m s}^{-1}$  in Experiment IS, while they are slightly stronger in Experiments G and PS, and more than  $6 \text{ m s}^{-1}$  in Experiment G, on account of the larger low-level inflow generated by the orography. Note that in all three island experiments, the low-level cyclone extends way out over the sea. In Experiment PNS, the

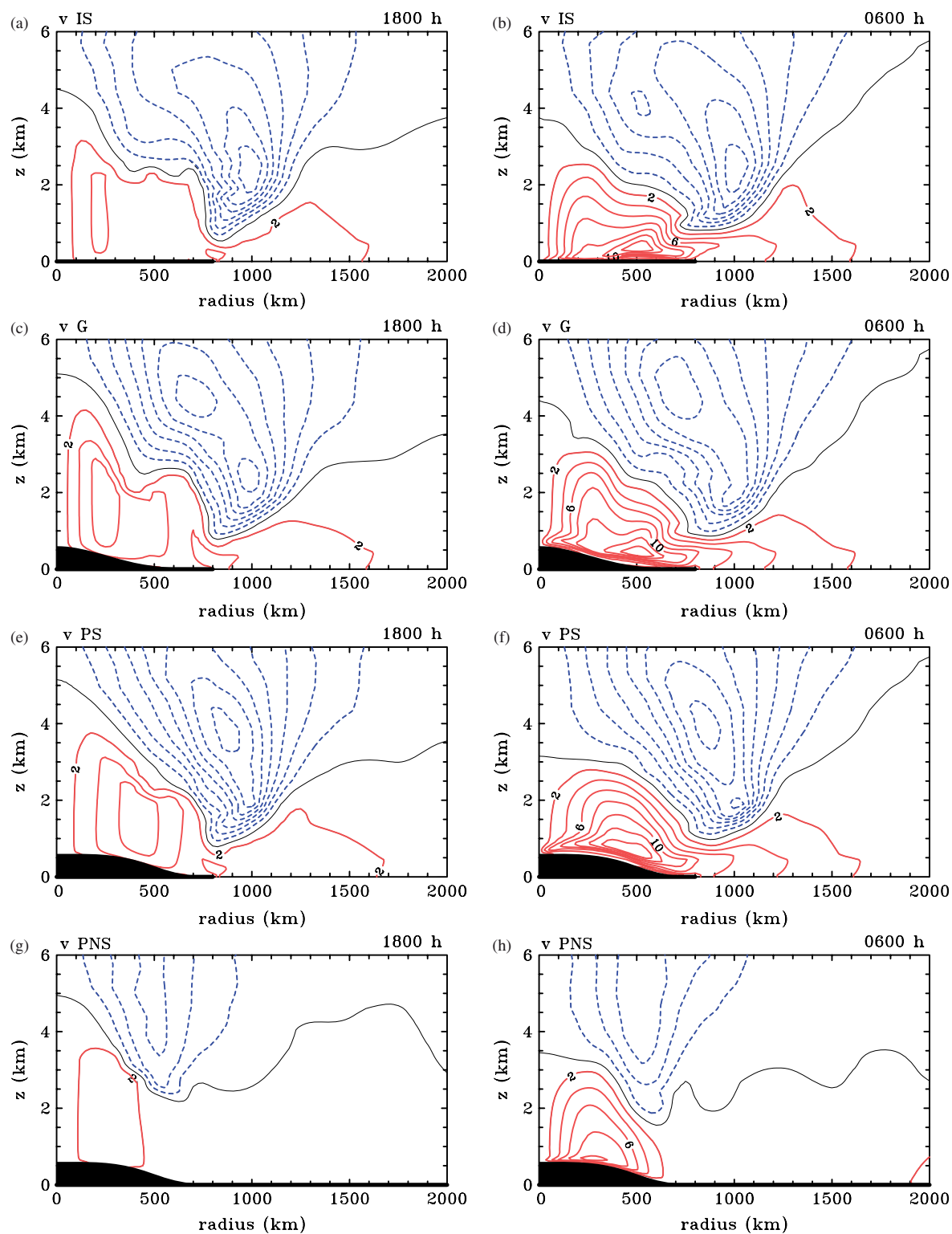


**Figure 7.** As Figure 3, but showing isotachs of the tangential wind component at (a, c, e, g) 1800 h and (b, d, f, h) 0200 h. The contour interval is  $2 \text{ m s}^{-1}$ , with positive contours (solid) representing cyclonic flow, and negative contours (dashed) representing anticyclonic flow. This figure is available in colour online at [wileyonlinelibrary.com/journal/qj](http://wileyonlinelibrary.com/journal/qj)

maximum tangential wind speed at 1800 h is weaker than in the island experiments, being less than  $4 \text{ m s}^{-1}$ . By 0600 h the tangential wind speed has increased to over  $10 \text{ m s}^{-1}$  in Experiments IS and PNS, over  $14 \text{ m s}^{-1}$  in Experiment G, and over  $16 \text{ m s}^{-1}$  in Experiment PS.

The low-level cyclone is surmounted by an anticyclone, which is associated with the divergent branch of the overturning circulation in conjunction with the approximate

conservation of absolute angular momentum. Aspects of the formation and evolution of the anticyclone are discussed in SS08 for the flat island case. As in this case, *the strength of the upper anticyclone in the presence of orography has a much smaller diurnal variation than the low-level cyclone.* This feature is evident in Figure 8(b), which shows the maximum and minimum values of the tangential wind component.

The effects of orography on the tangential circulation may be understood in terms of the differences in the strength and radial structure of the overturning circulation resulting from the orography. Some points to note are as follows.

Because the maximum slope of the orography is further from the centre of the island in Experiment PS than in Experiment G, the innermost inflow maximum at 1800 h is weaker than that in Experiment G, but the strength of the low-level cyclone is similar and it remains so during the night (Figure 8(a)). Clearly, there is not an exact one-to-one relationship between the maximum strength of the inflow and that of the low-level cyclone. This lack is to be expected and follows from the underlying principle highlighted in Smith *et al.* (2009) in a tropical-cyclone context. These authors showed that the spin-up of the low-level cyclone is the sum of two competing effects: (i) the inward displacement of air parcels as they partially conserve their absolute angular momentum; and (ii) the amount of absolute angular momentum lost during the displacement. While the radial displacement may be roughly characterized by the maximum radial velocity, it depends in detail on the distribution of radial velocity, i.e. how long the air parcel remains in the region of strong winds. Moreover, the more rapidly an air parcel converges, the less is the angular momentum lost by the frictional torque.

The stronger overturning circulation in Experiments G and PS leads also to a slightly stronger outflow and hence a slightly stronger upper-level anticyclone (maximum wind speed about  $15 \text{ m s}^{-1}$ ) at 0600 h than in Experiment IS. The value in Experiment PS is about  $2 \text{ m s}^{-1}$  larger than those for Experiments IS and G, where the maxima are almost identical (Figure 7(b)).

A notable feature of most experiments is the existence of a double maximum in the strength of the upper anticyclone at night and sometimes in the daytime. It is especially evident at 0600 h in Figures 7(b) and (f), but barely evident in Figure 7(d). It is even evident at 1800 h in Figure 7(c). We attribute these maxima to the occurrence of two prominent maxima in the radial outflow. One of these is anchored near the coast at a height of about 2 km and is clearly associated with the seaward branch of the sea breeze circulation. The other is associated with the seaward branch of the broad-scale overturning circulation, typically located inland at a height of around 4 km at 0600 h. This second maximum is prominent at 0600 h in Figures 5(d) and (f) and also in the Gaussian orography case at 1800 h (Figure 5(c)). However, it is not apparent at 0600 h in the flat island case (Figure 5(b)), but is a clear feature in this case earlier in the night, e.g. at 0200 h (not shown). In some cases and at some times, the upper maximum in the anticyclonic flow, which lies a little above 4 km, is the dominant one (e.g. Figures 7(c) and (d)), while in other cases and at other times, the lower maximum dominates (e.g. Figure 7(b)). The reason for the variability is that the higher-level outflow maximum is intimately connected with the gravity waves generated by the sea breeze, the phase of which moves downwards with time although the waves transfer energy upwards.

#### 4.4. The diurnal cycle

We turn now to examine time series of the minimum surface pressure at the domain centre and the maximum and minimum tangential wind component in the first five calculations listed in Table I. These time series are shown

in Figure 8. A prominent feature of all the calculations is the large diurnal variation in the low-level cyclonic circulation (Figure 8(a)). The largest tangential wind occurs in the experiments with orography and a surrounding sea (specifically Experiments G, PS, and WP), the maximum being about  $17 \text{ m s}^{-1}$  between 0200 h and 0500 h. The maximum in the flat island case is a little less, about  $15 \text{ m s}^{-1}$  and occurs slightly later, at about 0600 h. The low-level cyclone is weakest when there is no surrounding sea, the maximum tangential wind speed being only  $12 \text{ m s}^{-1}$ . In all cases the cyclone weakens during the daytime and re-strengthens again at night. The behaviour at low levels is in stark contrast to that aloft, where there is only a very weak diurnal variation in the strength of the anticyclone (on the order of  $1 \text{ m s}^{-1}$ ).

The maximum anticyclonic wind lies in most cases between  $12$  and  $17 \text{ m s}^{-1}$ , the exception being the plateau without a surrounding sea, which has a maximum of about  $6 \text{ m s}^{-1}$ .

The minimum surface pressure occurs at the centre of the island and has a diurnal range of 1.4–2 hPa in the cases with orography surrounded by sea, about 1.2 hPa in the case of the flat island, and only 1 hPa in the case of the plateau without a surrounding sea.

#### 4.5. Lower plateau height and the Saharan heat low

Three final calculations were designed to determine the sensitivity of the heat low to the height of the plateau (Experiments SPS and SPNS) and to provide an idealized flow configuration (Experiment GR) aimed at understanding the so-called ‘Atlantic inflow’, a concept introduced by Grams *et al.* (2010) to explain features of their observations and numerical simulation of the Saharan heat low. These authors describe the Atlantic inflow as ‘a complex mesoscale feature in western Mauritania’, the main components of which are ‘the sea breeze and associated front’ and ‘a marked baroclinic zone’. They state that ‘the baroclinic zone in the low and mid levels east of the sea breeze front marks the transition from the maritime-influenced atmosphere at the coastal region towards the Saharan atmospheric boundary layer/monsoon layer’, but they do not discuss the possible role of orography in establishing this baroclinic zone. In contrast, the solutions described above indicate that orography may be not only important, but may be the dominant effect in establishing the baroclinic zone seen in their experiments. The experiment to be described now supports this idea.

When the height of the orography in Experiments PS and PNS is reduced, so is the radial potential temperature contrast of the mixed layer over land (compare Figure 9 with Figure 3). Because of the lower radial gradient of potential temperature, the strength of the heat low, as measured by the maximum cyclonic wind speed (Figure 10), or by the minimum pressure at the domain centre (not shown), is reduced slightly. Nevertheless, the overall thermal patterns and flow patterns in Experiments SPS and SPNS are essentially the same as those in Experiments PS and PNS, respectively.

It may be noticed in Figure 9 that the phase of the diurnal surface pressure variation at the centre of the domain in Experiment PNS is different from that in all the island experiments. We have not explored this difference in depth, but the phase of the surface pressure having a minimum

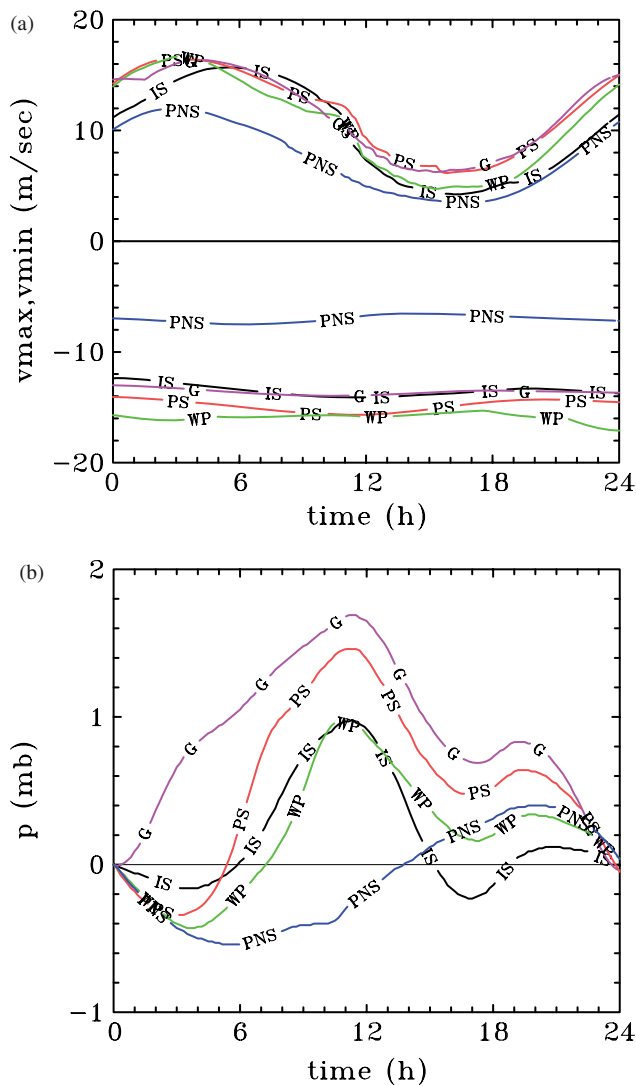


**Figure 8.** Time series of (a) the maximum and minimum tangential velocity over the whole domain, and (b) the surface pressure at the domain centre, in Experiments IS, G, PS, PNS and WP. This figure is available in colour online at [wileyonlinelibrary.com/journal/qj](http://wileyonlinelibrary.com/journal/qj)

at about 0600 h and a maximum at about 2000 h appears to be associated with a vertical wavenumber 1<sup>||</sup> standing gravity-wave oscillation in the mature stage of the flow evolution. The maximum surface pressure in the evening is accompanied by cooling through a deep layer in the vicinity of the axis associated with a deep layer of ascent.

The orography in Experiment GR was designed to have similar characteristics to the cross-section at 18°N over West Africa studied by Grams *et al.* (2010), including the lower sea-surface temperature used by them i.e. 20 °C. Compared with Experiment SPS, the orography is steeper, and the plateau and coastal plain are both slightly broader (Figure 1).

Grams *et al.* (2010) show a schematic of what they term ‘Atlantic inflow modes’ along their cross-section. In general the flow patterns in Experiment GR are similar to those in Experiment SPS, the most prominent differences being that the vertical velocities induced by the steeper terrain are stronger, and the sea breeze is a little stronger also on account of the slightly lower sea-surface temperature. The potential temperature at the domain centre is slightly higher than in

<sup>||</sup>At least wavenumber 1 within the domain shown in the figure.

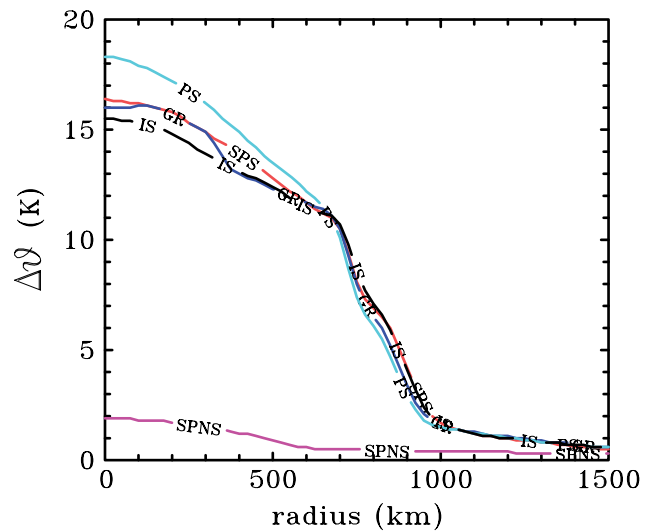


**Figure 9.** Radial profiles of the potential temperature difference,  $\Delta\theta$ , between the axis and far radial boundary at a height of 1500 m at 1800 h in the Experiments IS, PS, SPS, SPNS, and GR (defined in Table 1). This figure is available in colour online at [wileyonlinelibrary.com/journal/qj](http://wileyonlinelibrary.com/journal/qj)

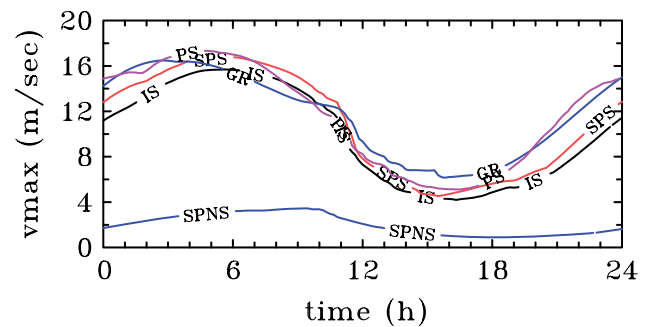


**Figure 10.** Time series of the maximum tangential velocity in Experiments IS, PS, SPS, GR, and SPNS (defined in Table 1). This figure is available in colour online at [wileyonlinelibrary.com/journal/qj](http://wileyonlinelibrary.com/journal/qj)

Experiment SPS also, presumably because there is a slightly broader plateau region and therefore a broader elevated heat source. Tests have shown that the 4 °C reduction in sea-surface temperature has relatively minor impact on the solutions.

Figure 11 shows radius–height cross-sections of potential temperature and vertical velocity in Experiment GR at 1800 h. Prominent features in Figure 11(a) are the broad-scale baroclinic zone over the land that is clearly enhanced over the slope of the orography, and the stronger baroclinic zone near the coast, which is associated with the sea breeze. These two features correspond with strong signatures in the vertical velocity pattern at 1800 h shown in Figure 11(b). The sea breeze is marked by a dipole pattern of strong ascent just inland from the coast and an elevated region of descent on the seaward side. A second dipole-like pattern of vertical motion is seen over and seawards of the orographic slope. Animations of the vertical velocity cross-sections at 10 min intervals show that both these dipole features move inland during the evening and that they are the lowest portions of upward-propagating gravity waves, with phase lines sloping inwards with height. As in Experiment PNS, the potential temperature gradient in Experiment SPNS is concentrated over the slope of the orography, i.e. the absence of sea isolates the effect of the orographic slope on the local

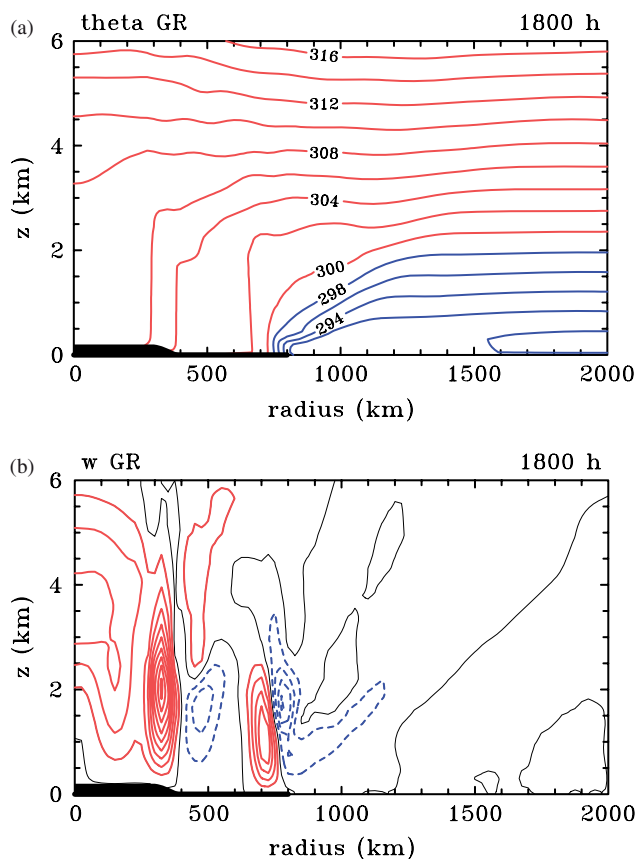


**Figure 11.** Radius–height cross-section of (a) potential temperature (contour interval 2 K), and (b) vertical velocity (contour interval  $1 \text{ cm s}^{-1}$ ) in Experiment GR at 1800 h. Contours with values less than 300 K, characteristic of air at low levels over the sea, are in bold (blue in the colour version). This figure is available in colour online at [wileyonlinelibrary.com/journal/qj](http://wileyonlinelibrary.com/journal/qj)

potential temperature of the mixed layer (Appendix B). The results of the three idealized experiments described in this section support the idea that the ‘Atlantic inflow’ or ‘Atlantic inflow modes’ described by Grams *et al.* (2010) are a superposition of the evolving sea breeze circulation and the evolving circulation associated with the broad-scale baroclinic zone over the land, but they show further that the horizontal thermal gradient is enhanced in the regions of orographic slope. Our calculations show also that the transient circulations excite upward-propagating gravity waves that are additional components of the ‘Atlantic inflow modes’ as defined by Grams *et al.* (2010).

#### 4.6. Comparison with RS03

A quantitative comparison of the present calculations with those of RS03 for Experiments PS and PNS broadly confirm the results shown by RS03 for these two experiments, although there are some differences over the sea. Unlike in the present calculations, both the tangential and overturning circulations in RS03 extend over the entire plotting domain with significant wind speeds out to radial distances of 4000 km. The difference is probably because RS03 applied the radiation scheme only over land and used an initial far-field vertical temperature profile that is not in radiative equilibrium. Both shortcomings explain why the slope of the isentropes in their Figure 10(a) reach all the way to the boundary. The presence of such a slope, which is absent in

the new calculations, explains the far-reaching circulation in the RS03 experiments.

## 5. Conclusions

We have investigated the effects of orography on the dynamics of a heat low that forms over a circular plateau surrounded by either sea or flat land. Several prominent features of the simulations with orography are similar to those over a flat island. These features include the large diurnal variation in the low-level winds, with the weakest winds in the afternoon and the strongest winds overnight. The differences in wind strength reflect the strong turbulent mixing of momentum in the mixed layer over land during the afternoon, which leads to a significant weakening of the cyclone circulation, and the formation of a strong low-level jet at night, which produces convergence towards the centre of the heat low. The Coriolis force associated with the inflow re-amplifies the tangential circulation. In contrast, the upper anticyclone, which lies above the mixed layer, undergoes a much weaker diurnal variation.

There is a prominent diurnal cycle in the vertical motion with mostly ascent over the land during the afternoon and evening and subsidence in the morning. In addition, there is a local pattern of ascent and descent that moves inland with the sea breeze. The phase tilt of this pattern with height is indicative of an upward-propagating gravity wave. Over the land there is a broad-scale negative radial gradient of potential temperature in the mixed layer. This baroclinicity results in an overturning circulation that extends through much of the lower troposphere. There is a large radial gradient of potential temperature in a shallower layer near the coast associated with the sea breeze front, which produces a shallower, but more intense, overturning circulation.

The presence of orography on the island enhances the strength of the broad-scale baroclinic zone and thus that of the overturning circulation. Steep orography leads to prominent localized enhancements. We showed that, as the height of the orography increases and the surface pressure decreases, the mixed-layer temperature increases monotonically because the surface heating is distributed over a column of lighter air. In the absence of a surrounding sea, the baroclinic zone is entirely a result of the orographic slope and both the overturning circulation and tangential circulation are closely tied to the slope.

Our calculations reveal only a weak sensitivity of the heat low intensity to a reduction in sea-surface temperature from  $24^\circ\text{C}$  to  $20^\circ\text{C}$ .

The idealized numerical experiments discussed herein provide a refined framework for understanding many of the observed features of heat lows in general and the Saharan heat low in particular. The latter is an important aspect of the climate of northwestern Africa and has attracted much recent interest. The results provide a refined basis for understanding the observed strong diurnal cycle in the West African monsoon winds with the strongest winds during the night and calm conditions during the daytime Parker *et al.* (2005). They support also the interpretation of the so-called ‘Atlantic inflow to the Saharan heat low’, described by Grams *et al.* (2010), as a superposition of the evolving sea breeze circulation and the evolving circulation associated with the broad-scale baroclinic zone over the land. However, they go further by highlighting the important role of orographic slopes in enhancing the baroclinicity inland

of the sea breeze. The transient sea breeze circulation excites upward-propagating gravity waves that are features also of the 'Atlantic inflow modes' described by Grams *et al.* (2010).

## Appendix A

### The errors in RS03

While the main error in the RS03 calculation lies in the radiation scheme discussed in section 3, there are two errors in the island calculations that do not appear to be serious, except possibly for the Gaussian-shaped orography, but are nonetheless worth documenting.

Firstly, for the island cases, RS03 did not set the pressure equal to the mean-sea-level pressure over the sea, but rather to that at height  $h(r)$ . Hence the pressure values just offshore are slightly underestimated and the pressure gradient between land and ocean is slightly overestimated. Furthermore, a weak surface pressure gradient is introduced over the sea. The largest effect occurs in the case of the Gaussian-shaped orography where the height of the orography at the coast is 66.2 m and the pressure difference 7.6 hPa. In the other island cases (PS/PNS and WP) the heights of the orography at the coast are 5.5 m and 7.3 m, respectively, corresponding with pressure differences 0.64 hPa and 0.85 hPa.

Secondly, the initial temperature distribution was chosen in a way that each  $\sigma$ -level was assigned a constant temperature, where temperature decreases as  $\sigma$  decreases. Since orography displaces the  $\sigma$ -levels vertically, one has to take into account a reduction of temperature over the mountain on constant  $\sigma$ -surfaces. This specification initiates a circulation with upslope flow and divergence above the mountain that will contaminate the solution at early times. However, it should not appreciably affect the mature state, which was the focus of RS03's discussion.

## Appendix B

### Dependence of differential net heating on surface pressure

An increase in height of the orography was argued to yield higher potential temperatures of the mixed layer based on a reduced mass, i.e. a lower surface pressure, being exposed

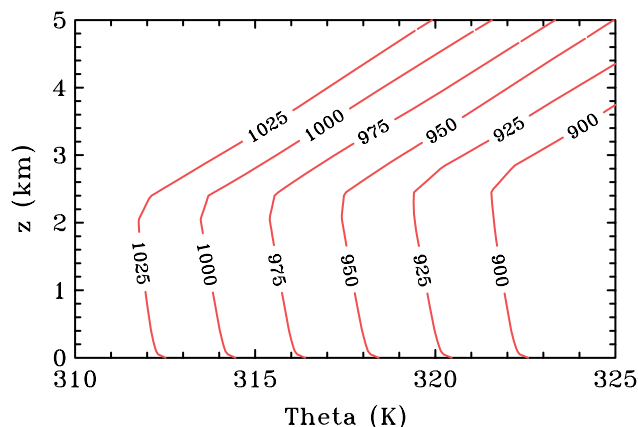


**Figure B1.** Vertical profiles of potential temperature at 1800 h obtained from the one-dimensional version of the model for different surface pressures (indicated in hPa on each curve). This figure is available in colour online at [wileyonlinelibrary.com/journal/qj](http://wileyonlinelibrary.com/journal/qj)

to the identical solar heating input. To test the dependence of the mixed-layer potential temperature on the surface pressure, a one-dimensional version of the numerical model was integrated, initialized with different surface pressures. The model was integrated for 30 d to reach a repeating diurnal cycle. Figure B1 shows the potential temperature of the lower 5 km for surface pressures varying between 900 hPa and 1025 hPa in 25 hPa increments. The increase in potential temperature of the mixed layer with decreasing surface pressure is clearly discernible. The mixed-layer depth increases only slightly with decreasing surface pressure, while the stratification above the mixed layer appears to be unchanged.

## Acknowledgements

We thank Doug Parker and an anonymous reviewer for their perceptive comments on the original manuscript.

## References

- Adams M. 1986. A theoretical study of the inland trough of northeastern Australia. *Aust. Meteorol. Mag.* **34**: 85–92.
- Adams M. 1993. A linear study of the effects of heating and orography on easterly airstreams with particular reference to northern Australia. *Aust. Meteorol. Mag.* **42**: 69–80.
- Alonso S, Portela A, Ramis C. 1994. First considerations on the structure and development of Iberian thermal low-pressure system. *Ann. Geophys.* **12**: 457–468.
- Emanuel KA, Neelin JD, Bretherton CS. 1994. On large-scale circulations in convecting atmospheres. *Q. J. R. Meteorol. Soc.* **120**: 1111–1143.
- Fandry CB, Leslie LM. 1984. A two-layer quasi-geostrophic model of summer trough formation in the Australian subtropical easterlies. *J. Atmos. Sci.* **41**: 807–818.
- Fitzjarrald DR, Garstang M. 1981. Vertical structure of the tropical boundary layer. *Mon. Weather Rev.* **109**: 1512–1526.
- Gaertner MA, Fernandez C, Castro M. 1993. A two-dimensional simulation of the Iberian summer thermal low. *Mon. Weather Rev.* **121**: 2740–2756.
- Grams CM, Jones SC, Marsham JH, Parker DJ, Haywood JM, Heuveline V. 2010. The Atlantic inflow to the Saharan heat low: Observations and modelling. *Q. J. R. Meteorol. Soc.* **136**: 125–140.
- Hoinka KP, Castro M. 2003. The Iberian peninsula thermal low. *Q. J. R. Meteorol. Soc.* **129**: 1491–1511.
- Johnson RH. 2003. Thermal low. *Encyclopedia of Atmospheric Science*. Holton J, Pyle J, Curry JA. (eds) Academic Press: London.
- KePERT JD, Smith RK. 1992. A simple model of the Australian west coast trough. *Mon. Weather Rev.* **120**: 2042–2055.
- Lafore JP, Flamant C, Giraud V, Guichard F, Knippertz P, Mahfouf J-F, Mascart P, Williams E. 2010. Introduction to the AMMA special issue on 'Advances in understanding atmospheric processes over West Africa through the AMMA field campaign'. *Q. J. R. Meteorol. Soc.* **136**(S1): 2–7. DOI: 10.1002/qj.583.
- Leslie LM. 1980. Numerical modelling of the summer heat low over Australia. *J. Appl. Meteorol.* **19**: 381–387.
- Leslie LM, Skinner TCL. 1994. Real-time forecasting of the western Australian summertime trough: Evaluation of a new regional model. *Weather Forecast.* **9**: 371–383.
- Mellor G, Yamada T. 1974. Hierarchy of turbulence closure models for planetary boundary layer. *J. Atmos. Sci.* **31**: 1791–1806.
- Mellor G, Yamada T. 1982. Development of a turbulent closure model for geophysical fluid problems. *Rev. Geophys. Space. Phys.* **20**: 851–875.
- Parker DJ, Burton RR, Diongue-Niang A, Ellis RJ, Felton M, Taylor CM, Thorncroft CD, Bessemoulin P, Tompkins AM. 2005. The diurnal cycle of the West African monsoon circulation. *Q. J. R. Meteorol. Soc.* **131**: 2839–2860.
- Portela A, Castro M. 1996. Summer thermal lows in the Iberian peninsula: A three-dimensional simulation. *Q. J. R. Meteorol. Soc.* **122**: 155–163.
- Preissler M, Reeder MJ, Smith RK. 2002. A case study of a heat low over central Australia. *Aust. Meteorol. Mag.* **51**: 155–163.
- RÁCZ Z, Smith RK. 1999. The dynamics of heat lows. *Q. J. R. Meteorol. Soc.* **125**: 225–252.

- Raymond DJ. 1994. Convective processes and tropical atmospheric circulations. *Q. J. R. Meteorol. Soc.* **120**: 1431–1455.
- Redelsperger JL, Thorncroft CD, Diedhiou A, Lebel T, Parker DJ, Polcher J. 2006. African Monsoon Multidisciplinary Analysis: An international research project and field campaign. *Bull. Amer. Meteorol. Soc.* **87**: 1739–1746.
- Reichmann Z, Smith RK. 2003. Terrain influences on the dynamics of heat lows. *Q. J. R. Meteorol. Soc.* **129**: 1779–1793.
- Smith RK, Vogl S. 2008. A simple model of the hurricane boundary layer revisited. *Q. J. R. Meteorol. Soc.* **134**: 337–351.
- Smith RK, Montgomery MT, Nguyen VS. 2009. Tropical cyclone spin-up revisited. *Q. J. R. Meteorol. Soc.* **135**: 1321–1335.
- Spengler T, Smith RK. 2008. The dynamics of heat lows over flat terrain. *Q. J. R. Meteorol. Soc.* **134**: 2157–2172.
- Spengler T, Reeder MJ, Smith RK. 2005. The dynamics of heat lows in simple background flows. *Q. J. R. Meteorol. Soc.* **131**: 3147–3166.
- Thorncroft CD, Blackburn M. 1999. Maintenance of the African easterly jet. *Q. J. R. Meteorol. Soc.* **125**: 763–786.
- Ulrich W, Smith RK, Nguyen C. 2002. Comparison of an axisymmetric hurricane model with the corresponding slab-symmetric ITCZ model. *Q. J. R. Meteorol. Soc.* **128**: 2335–2347.
- Zängl G, Chico SG. 2006. The thermal circulation of a grand plateau: Sensitivity to the height, width, and shape of the plateau. *Mon. Weather Rev.* **134**: 2581–2600.